Analysis of Time Delays in the Gravitational Lens PG1115+080

Rennan Bar-Kana[1]
Physics Dept. Rm. 6-218M, MIT, 77 Massachusetts Ave, Cambridge, MA 02139 USA

ABSTRACT

We present a new method for determining time delays among the light curves of various images in a gravitational lens. The method is based on constructing a simple model for the source variation and forming a χ^2 measure of the agreement of this same variation with all of the lightcurves. While inspired by Press et al. (1992a, b) our approach is different since we do not assume a Gaussian process for the source variation. Our method has a number of desirable properties: first, it yields an approximate reconstruction of the source variation and of other parameters such as relative time delays; second, it easily incorporates different assumptions about the relations among the light curves and about the data measurement errors; finally, it can be applied to more than two light curves by addition of χ^2. We apply this method to the light curves of the quadruple gravitational lens PG1115+080 measured by Schechter et al. (1997). Unlike Schechter et al. we include correlated measurement errors in the analysis, as well as the possibility that microlensing may cause different images to vary by different factors in flux. We find a value of $25.0^{+3.3}_{-3.8}$ days (95% confidence) for the delay between components B and C (close to the 24 day value of Schechter et al., and so leading to a similar value of the Hubble constant for a given lens model). However, the ratio t_{AC}/t_{BA} of the two intermediate delays is poorly determined at $1.13^{+.18}_{-.17}$ (68% confidence), close to the value predicted by lens models (~ 1.4) unlike the Schechter et al. value (~ 0.7). The variation ratios of C with respect to A and of A with respect to B are both different from 1, $1.39^{+.16}_{-.20}$ and $.79^{+.10}_{-.12}$ (95% confidence), respectively. This is an indication of a microlensing gradient, and this type of microlensing may allow us to conclude that the size of the quasar optical emission region is about 1000 AU.

Subject headings: cosmology — distance scale — gravitational lensing

1. Introduction

Even before the discovery of the first gravitational lens 0957+561 (Walsh, Carswell & Weymann 1979) it was recognized that measurements of the time delay between images can be used to determine the Hubble constant (Refsdal 1964, 1966). Despite a history of systematic difficulties, recent measurements combined with an analysis of lens models (Grogin & Narayan 1996a, 1996b) indicate that a robust

[1]email: barkana@arcturus.mit.edu

measurement of the Hubble constant (H_0) with an accuracy comparable to that of more conventional techniques may be within reach. The measurements include a precise optical time delay (Kundić et al. 1997) which is consistent with the latest results from radio monitoring (Haarsma et al. 1997), and a measurement of the velocity dispersion of the lens galaxy (Falco et al. 1997).

Since each lens can potentially yield an independent, single step H_0 measurement, obtaining values in a number of lenses with a variety of morphologies and constraints on models may help eliminate systematic errors. Each lens requires a well-constrained lens model, lens and source redshifts, and a measurement of the time delays among the images. Observational constraints on the lens model may include precise image positions and flux ratios as well as data on the objects responsible for the lensing. Resolved structure in images as revealed by radio interferometry provides many constraints, since it is essentially the same as observing multiple sources with the same lens. Whether lensing involves a galaxy, group, or cluster, the position, velocity dispersion, and other observational probes of the mass distribution of the lensing objects all yield constraints on lens models. Measuring time delays requires observing time variations in the image intensities with sufficient accuracy and time resolution. As the number of lenses being carefully monitored increases, more time delays are being determined, such as the preliminary measurement in PKS 1830-211 (Van Ommen et al. 1995). Flux measurements are not the only possibility, as shown by the promising measurements of variations in polarization fraction in the images of B 0218+357 (Corbett et al. 1996).

The quadruply imaged quasar PG1115+080 was the second lens to be discovered (Weymann et al. 1980). It is radio quiet, but optical Hubble Space Telescope images (Kristian et al. 1993) were recently analyzed by Schechter et al. (1997, hereafter SCH) and by Keeton & Kochanek (1997). They found that lens models which include the effect of the lens galaxy and that of the nearby group of galaxies discovered by Young et al. (1981) can fit the image positions well. They however still found great freedom in the H_0 values predicted by these lens models for a given time delay.

In four-image configurations where the images lie at roughly the same distance from the lens, there is a well known degeneracy between the radial profile of the lens mass and the inferred H_0 (Kochanek 1991; Wambsganss & Paczyński 1994). In this situation the relative image positions do determine the total enclosed mass within the ring of images, but they are not very sensitive to the radial profile of the mass. Changing the radial profile affects the convergence at the images, and this changes the inferred H_0 value in a similar way to the effect of a constant mass sheet (Falco et al. 1985; Narayan 1991). In PG1115+080 future observations of the lensing galaxy light profile and, ultimately, a direct measurement of its central velocity dispersion may constrain or eliminate this degeneracy.

Recently SCH measured light curves for the A1, A2, B and C images of PG1115+080, and used them to determine multiple delays. The bright A1 and A2 images are close together and should have a very small time delay ($\sim$ a few hours), so they were combined into a single A=A1+A2 curve. SCH used the Press et al. (1992a, b) method and found that C leads A and A leads B, with $t_{BC} = 23.7 \pm 3.4$ days and $t_{AC} = 9.4 \pm 3.4$ days which yields a ratio $r_{ABC} \equiv t_{AC}/t_{BA}$ of 0.7 ± 0.3. It is useful to express the two independent quantities as t_{BC} and r_{ABC}, since t_{BC} can be taken to fix the Hubble constant for a given lens model while r_{ABC} is independent of overall distance, and can be compared directly with the ratio predicted by lens models. The models mentioned above are consistent in predicting $r_{ABC} = 1.4$ to within

about 0.1, and SCH noted the 2σ discrepancy with their fitted value. In their analysis SCH assumed that the measurement errors in the light curves are uncorrelated, and also that the fractional flux variations are the same for each component.

In this paper we present a more detailed analysis of the light curves in PG1115+080. We first present a new method based on χ^2 minimization, which has many of the advantages of Press et al. (1992a, b), but is simpler and allows for a more conservative assessment of errors in the reconstructed parameters. We then apply this method to PG1115+080, and include correlated measurement errors in the analysis. In addition to relative time delays, we also allow for different factors of variation in flux, which may arise from microlensing of the images. In §2 we present our χ^2 method, and discuss its distinct features and free parameters. We then discuss the physical meaning of the various parameters that the method can account for and attempt to extract from data. In §3 we apply our method to fitting the PG1115+080 light curves, singly, in pairs, and all together, and discuss the results and implications. Finally in §4 we summarize our results and point out some of the significant returns possible from further monitoring.

2. Method and physical parameters

Suppose we have a light curve of N points, (t_i, v_i) $i = 1, \ldots, N$, where t_i is time (in days) and v_i is the intensity (in magnitudes) at time t_i, and we construct a model for $v(t)$ with M adjustable parameters a_j, $j = 1, \ldots, M$. Then if the v_i measurements are independent, with normally distributed errors of standard deviation σ_i for each i, the χ^2 measure of goodness-of-fit is

$$\chi^2 = \sum_{i=1}^{N} \left[\frac{v_i - v(t_i; a_1 \ldots a_M)}{\sigma_i} \right]^2 \ . \tag{1}$$

When the measurement errors are correlated, with a covariance matrix $\mathbf{Q}$, then

$$\chi^2 = \sum_{i,j=1}^{N} W_{ij} \ [v_i - v(t_i; a_1 \ldots a_M)] \ [v_j - v(t_j; a_1 \ldots a_M)] \ , \tag{2}$$

where the weight matrix $\mathbf{W}$ is the matrix inverse of $\mathbf{Q}$.

We wish our model for $v(t)$ to be an arbitrary continuous curve. Although quasar variations may be stochastic, the variations typically decrease in amplitude at smaller and smaller time scales, and a continuous curve can describe the large time-scale variations well. Of course, we cannot take an *arbitrary* curve, since we must describe the curve with a small number of parameters. We therefore take L points (t_k, v_k) with the t_k just covering the range of the data and equally spaced. The v_k are then the parameters, and the model for $v(t)$ is a curve going through all the (t_k, v_k) with interpolation used for other values of t. Note that we interpolate between the v_k in the model, only as a way of parameterizing a general curve $v(t)$ in terms of the L parameters; we do not interpolate between the noisy data points directly. When we fit multiple light curves, a single such model is used for all of them, or equivalently the light curves are all combined into a single light curve which is then compared to the model. Additional parameters can be added to account for relative shifts of an entire light curve relative to the others, before comparing

to the model. A relative magnification corresponds (in magnitudes) to adding a constant to all the measured v_i of an image. A relative time delay corresponds to adding a constant to all the measured t_i of an image. For given time delays, all the other parameters are linear (i.e. the χ^2 is a quadratic form in these parameters) if we use only interpolation which is linear in the v_k (but arbitrarily non-linear in the t_k). Minimizing the χ^2 then corresponds to solving a linear system, and we solve it using Cholesky decomposition (e.g. Press et al. 1992c, §2.9).

Like Press et al. (1992a, b), our method compares a model for the source variation to the light curves with a χ^2 measure, and thus both methods assume that the statistics of the measurement errors are Gaussian. However, the two methods construct the model of the source variation very differently. In Press et al. the source variation is assumed to be a stationary Gaussian process, with a correlation function which is extracted from the light curves themselves. In that method there is some freedom to vary the assumed correlation function in order to check for robustness. In our method we assume no particular form for the correlations among source fluxes at different source times. By taking a continuous curve we are effectively smoothing the actual source variation over some small time scale, but the curve is otherwise arbitrary. Although the two methods use different assumptions, they may not necessarily yield very different results, since the intrinsic variability of quasars appears to decrease at small time scales. Qualitatively, then, both methods are dominated by requiring smoothness for nearby points when all the light curves are combined. We also note that the correlations which we *are* including are in the observational errors of different images observed at a single time. Such correlations were not accounted for by SCH, but they in principle can also be included in the Press et al. method.

Our model is very flexible. There is freedom to choose both the number of interpolation points L and the interpolation method. We use several methods of interpolation. Given some time t between (t_k, v_k) and (t_{k+1}, v_{k+1}), in linear interpolation we take for $v(t)$ the linearly interpolated value between v_k and v_{k+1}. In cubic interpolation we interpolate using the cubic polynomial through the four points at $k-1$, k, $k+1$ and $k+2$ (with linear interpolation used for $k=1$ or $k=L-1$). In cubic spline interpolation (e.g. Press et al. 1992c, §3.3), we draw a cubic polynomial between every pair of points k and $k+1$ so that the entire curve is continuous in the second derivative. We find in §3 below that changing the interpolation method has a rather minor effect. Note that with any of these interpolation methods there is some inter-dependence among all of the v_k, unless there is some k_0 with no data points between t_{k_0} and t_{k_0+1}. In this case the parameters v_k for $k > k_0$ would decouple from those with $k < k_0$, at least with linear interpolation. There are 37 points in each light curve in the PG1115+080 data, and the final data point follows a gap of 38 days. Hereafter we drop this last point, and then we are never in a situation where such a k_0 exists (The above argument suggests that the last point has only a small effect on the results with our method, and this is indeed the case).

The number of points in each light curve is thus 36, and we use an L of 10, 20 and 30. Below we find that the differences in the derived parameters using the various L are fairly large, so this freedom provides a more conservative and robust estimate of parameter uncertainties. Using small L corresponds essentially to a larger-scale smoothing of the data, though once again the smoothing is not directly of the raw data. If we use a very small L, we are over-smoothing the signal, and we may expect an unreliable reconstruction if the actual signal is not smooth enough on timescales $\leq \Delta T/L$, where ΔT is the total

length of the data. If on the other hand we use a large L, there are fewer constraints on the v_k, and we may get large oscillations between nearby v_k as the fitting procedure tries to compensate for individual measurement errors. Using a range of L thus allows an important check on robustness, and in some sense checks for systematic errors over and above the statistical errors on the results for a given L.

When we use a method based on χ^2 minimization for finding time delays among a number of curves, we may worry about being biased towards large time delays. This is because large time delays imply little overlap among the light curves, and so smaller χ^2 since there are fewer constraints coming from requiring smoothness when the light curves are combined into a single curve. In our method, with a fixed L, this bias is partially offset since larger time delays imply larger effective smoothing as the total ΔT for the combined light curves increases. In practice we find negligible bias in the Monte Carlo tests described in §3 below.

We wish to also account for the effect of microlensing in the fitting. Microlensing is the additional magnification of each image due to lensing by stars or dark matter clumps in the lensing galaxy. In 2237+0305 microlensing on the scale of months was first detected by Irwin et al. (1989) and confirmed by Houde & Racine (1994). Such microlensing has also been detected in 0957+561, with indications of possible microlensing on smaller time scales (Schild 1996). Microlensing may cause an amplification of order 0.6 magnitudes, which in PG1115+080 is expected to vary over a time scale (Witt et al. 1995) of ~ 10 years (If there is microlensing on a scale of days or weeks in PG1115+080, it appears to be small in the data, and we include it in the noise and not explicitly in the analysis). However, even if there is no significant variation over the span of the measured light curves, there may be a 'static' microlensing effect which causes different images to vary by different factors in flux, as suggested by SCH. This results from the fact that when we observe a quasar varying over time we may effectively be observing two different sources. If the flux variation results from a uniform brightening and dimming of the entire quasar emission source, then we are only observing a single source. However, if some portions of the emission region vary differently from other parts, then the region which produces the mean (i.e. time-independent part of the) flux is not identical to the region responsible for the small intensity variations with time. A possible physical picture is that the variation is caused by a small jet emanating from the core or a sudden localized surge of mass accretion.

In such a situation, the overall magnifications M_i of the mean flux F and m_i of the variation f may be unequal for a given image i, and their ratio m_i/M_i may be different for different images. In magnitudes, we would then measure (except for an overall factor of $-5/2$)

$$\log_{10}(M_iF + m_if) = \log_{10}(M_iF) + \log_{10}\left(1 + \frac{m_if}{M_iF}\right) \simeq \log_{10}(M_iF) + \frac{m_i}{M_i}\frac{f}{F\ \log 10}\ , \qquad (3)$$

where we assume $f/F \ll 1$. The variation in magnitudes may therefore have different amplitudes in different images if the m_i/M_i ratio is not the same for all i.

The spatial scale for microlensing is set by the Einstein radius of a typical deflector at the lens plane, projected onto the source plane. In PG1115+080 this radius is

$$\zeta_E = 5 \times 10^{-3}\ \left[\langle M\rangle /0.1M_\odot\right]^{1/2}\ \mathrm{pc} = 1000\ \left[\langle M\rangle /0.1M_\odot\right]^{1/2}\ \mathrm{AU}\ , \qquad (4)$$

where $\langle M \rangle$ is the average stellar mass (Witt et al. 1995). In order to have m_i and M_i not be equal, one or both of the emission regions must have structure on scales of order ζ_E or smaller: if they were both smooth then the microlensing would be washed out, and we would have $m_i = M_i$ for all i. On the other hand, if the two emission regions overlapped and their union had a very small extent compared to ζ_E, then the magnification due to microlensing would not vary over this scale, and again we would have $m_i = M_i$. Thus we reach the interesting conclusion that the indication of different m_i/M_i for different i (see §3 below) implies that the size of the quasar optical emission region *must be of order* ζ_E, say to within a factor of 10.

There are, however, a number of reasons to be cautious about this statement. The two emission regions may have different sizes, and in this case we might expect the mean region to contain the variation region, and then the different m_i/M_i would imply the lower bound only on the larger emission region. More generally, while there appears to be significant emission from a structure of size ζ_E, this does not exclude a range of structure also on smaller or larger length scales. In addition, ζ_E depends on what we assume for $\langle M \rangle$, and there could be a large range of masses contributing. The intensity variation may involve relativistic motions, and such high velocities can cause microlensing variations on small time scales that we might confuse as differences in m_i/M_i. The stochastic nature of optically-thick microlensing (e.g. Witt et al. 1995) implies the possibility of a rare statistical fluctuation over the relatively short time span of the current data. Note also that the magnification due to the macrolens itself varies with position, but it should only vary over much larger spatial scales. There could be a different amount of contamination by light from the lens galaxy in each image, and this would lead to apparent changes in the M_i with no corresponding changes in the m_i. However, in PG1115+080 this effect seems to be too small to affect the m_i/M_i ratios significantly. Finally, there may still be unmodelled systematic errors in the measured light curves which could give the appearance of unequal m_i/M_i ratios. With a longer time span of measurements it may be possible to eliminate some or all of these uncertainties. See also Gould & Miralda-Escudé (1997) for an independent, illuminating discussion of the possible observational consequences of differential microlensing of accretion disks in quasars. We note that the size given in equation (4) is roughly consistent with the upper limit from the interpretation of microlensing in 2237+0305 (Wambsganss, Paczynski & Schneider 1990). It is somewhat smaller than an estimate by Schild (1996) based on variations in 0957+561.

In measuring the quasar image light curves, SCH used two nearby stars, *B and *C, as photometric references. All intensities (i.e. for the images as well as for *B) were measured with respect to *C, and SCH then subtracted one half of the magnitude of *B from the quasar components, for each observation. The correlation between the quasar and *B may result from systematic errors such as the adopted point spread function, which varies across the field and so may not be identical in *B and in the quasar components. In our analysis we treat the fluctuations of *B as stochastic noise, with a component which is common to *B and to all the quasar components, as well as an independent source of error. We then let the χ^2 minimization decide the size of the error common to *B and all the quasar images, separately in each observation, but guided by our best estimate of the typical size of the correlation. Thus, we add *B to our method effectively as a fourth light curve, but for the underlying model of *B we take just a constant intensity in time. We also assume an error component common just to the three quasar images.

Note that such correlated errors are visually apparent from the data, e.g. in Figure 2 of SCH near days 100, 130, and 150, with the clearest example near day 90.

3. Results for PG1115+080

Our model for component A consists of L points as described in §2. For B we use the same model, but with an overall magnitude shift m_{BA} of A with respect to B (accounting for mean magnification), a time shift t_{BA} due to the time delay, and an overall variation ratio α_{BA} multiplying the variation (accounting for differential microlensing as explained in §2). Similarly, we have m_{AC}, t_{AC}, and α_{AC}, as well as m_{BC}, t_{BC}, and α_{BC}. When we fit all the curves simultaneously, we have the constraints $m_{BC} = m_{BA} + m_{AC}$, $t_{BC} = t_{BA} + t_{AC}$, and $\alpha_{BC} = \alpha_{BA}\alpha_{AC}$. The only parameters which require non-linear χ^2 minimization are t_{BA}, t_{AC}, α_{BA}, and α_{AC}. We minimize with respect to these parameters using direction set methods (Press et al. 1992c, §10.5).

We vary a number of parameters in the model. We try $L = 10$, 20 and 30 interpolation points. We try linear, cubic and cubic spline interpolation. For the measurement errors, we begin with the uncorrelated errors for A, B and C of 2.3, 7.5 and 4.0 millimagnitudes (mmag) at 1σ, respectively (SCH). We also take an uncorrelated error of 1.2 mmag for the bright star *B. We then add an error of standard deviation σ_n common to *B and all QSO components, and also separate errors of $f_1\sigma_n$ in *B and $f_2\sigma_n$ in all the QSO components. If we assume $f_1 = f_2 = 1$, then since *B has a measured variability of 8 mmag at 1σ, we take $\sigma_n \simeq 6$ mmag. As we show below, reasonable variations in σ_n, f_1 and f_2 affect the minimum χ^2 value but not appreciably values of the derived parameters such as the time delays. On the other hand, having no correlated errors at all ($\sigma_n = 0$) does change the derived parameters. All the errors are naturally assumed to be Gaussian in the χ^2 method.

We can also take Gaussian errors for Monte Carlo trials. On the other hand, since the method reconstructs a model for the input signal, it also reconstructs an estimate of the measurement errors in all the light curves in each observation. We take these actual errors instead of Gaussian errors for a second, bootstrap-like Monte Carlo analysis. Thus we have a set of 36 observations, and in the Monte Carlo trials for each day we pick one of the 36 at random (with replacement) and add the reconstructed errors on that day (in A, B, C, and *B) to the matching simulated light curves (i.e. A, B, C, and *B, respectively). Note that this is not a rigorous bootstrap, since after the χ^2 minimization the errors are no longer independent. However, this procedure should give us an idea of the actual size and mutual correlations of the measurement errors, and should be more robust and conservative than the Gaussian Monte Carlo trials. For the input signal in the Monte Carlo trials we take a smooth curve (see Figure 1) with roughly the same shape as the variation in the actual data. This way, the input is identical to the real signal on large time scales, and we assume that any apparent small scale variability is dominated by measurement noise, which seems likely.

We define our 'standard' model as having $L = 20$, cubic spline interpolation, $\sigma_n = 6$ mmag and

$f_1 = f_2 = 1$. Thus the assumed covariance matrix of errors for this model in mmag squared is

$$\begin{pmatrix} 77.3 & 72 & 72 & 36 \\ 72 & 128.3 & 72 & 36 \\ 72 & 72 & 88.3 & 36 \\ 36 & 36 & 36 & 73.3 \end{pmatrix} \tag{5}$$

with rows from the top in the order A, B, C, and *B. Hereafter we use these standard settings except where otherwise noted.

We begin by fitting each quasar component separately, always along with *B. Table 1 shows the resulting values of the χ^2 per degree of freedom $\bar{\chi}^2$, for various L. The number of data points is 72 (36 each for a quasar component and for *B), and the number of parameters is $L + 1$ (1 for the mean value of *B), which yields $71 - L$ for the number of degrees of freedom (ndof). The reduced χ^2 is in most cases less than 1, which is reasonable since we are assuming that a significant portion of the error is correlated among all the quasar components, and if we take each of them separately then we are not including this very strong constraint. Table 1 also suggests that if our error estimates are roughly correct for A and C, they may be somewhat underestimated for component B. Note that the $\bar{\chi}^2$ value is higher than 1 at $L = 10$ only for B, which is the faintest component and so has the largest errors. This may indicate higher non-Gaussianity for the errors in this component, since with lower L the fewer parameters cannot effectively compensate for outlier points.

Next we fit *B and two quasar components at a time, with the results displayed in Table 2. There are $36 * 3 = 108$ data points, and $L + 4$ parameters (e.g. *B mean, m_{BC}, t_{BC} and α_{BC}). Also shown are the one sided 68% confidence limits derived from 300 bootstrap Monte Carlo trials. Both the bootstrap errors and the parameters (t_{BC} etc.) that we input into the Monte Carlo trials are in each case (i.e. for each pair of components and for each L) set according to the values fitted from the data in that case. So e.g., for the BC pair with $L = 20$, a value of $t_{BC} = 25.3$ days is used as input for the Monte Carlo trials which in turn determine the error of $^{+2.3}_{-2.0}$ days on t_{BC}. We only show the results of varying L since this leads to the largest variations (see below). Note that the BA time delay has the largest fractional uncertainty, as we expect: B has the largest errors, so the uncertainty in t_{BA} is greater than in t_{AC}, and while C has larger errors than A, the BC delay is larger and much better resolved than is t_{BA}. For the variation ratios, there is some variation with L, but only α_{BC} is consistent with 1, while the others disagree with 1 at the $4 - 5\sigma$ level for each L.

Finally we combine all three quasar components, with results shown in Table 3. Uncertainties, where shown, are again one sided 68% confidence limits derived from bootstrap Monte Carlo trials. All the models are based on our standard inputs, except for the changes shown in the first column. In rows 4 and 5, σ_n is in mmag. In rows 6 and 7, f_1 and f_2 refer to assumptions about the correlated errors (see the beginning of this section). In rows 8 and 9, we use cubic and linear interpolation, respectively (see §2 above). As above, $r_{ABC} \equiv t_{AC}/t_{BA}$. We try a large range of model assumptions, most of which show very little variation in parameter values relative to varying L. The exception is the last row, marked 'SCH-like'. Here we use our method, but with assumptions that correspond closely to those of SCH: we assume no correlated errors, the uncorrelated errors are doubled, *B is not included in the fitting but

rather we subtract half of *B from the quasar light curves, and we set the variation ratios to 1. The 'SCH-like' parameter values are compatible with those of SCH to about 1σ.

A χ^2 method, in which errors are assumed to be Gaussian, can be sensitive to a small number of outliers. We use two procedures to check for the effects of such 'bad' measurements. First, we iteratively remove outliers. After fitting with our standard model parameters, we compare each point on every light curve to the reconstructed signal. We divide the difference by the individual uncorrelated error for that point, which yields the number of standard deviations that each point is off by. We add 20% to the error for points off by more than 4σ, and add 10% for points off by $2\sigma - 4\sigma$. We then fit with the adjusted errors, and repeat until convergence. The resulting values are $t_{BC} = 24.0$ days and $r_{ABC} = 1.15$, well within 1σ of the results from the standard fit. As a second check, we try fitting the time delays after removing points from the data set. We remove three points at a time, i.e. one point from each light curve, all taken in the same observation. This yields 36 sets of data. In two of these data sets we remove points from the first or last observation, thereby changing the total time span of the data and thus the model spacing for a fixed L. In order to avoid this, and to be able to check the effects of outliers independently from the effects of model spacing, we in fact do not explicitly remove any points, but rather multiply their individual errors by 1000 for a de facto removal. The 36 fits to these data sets yield a mean $t_{BC} = 25.1$ days with a standard deviation of 0.35 days, a minimum of 23.9 days and a maximum of 26.1 days. They also yield a mean $r_{ABC} = 1.13$ with a standard deviation of 0.03, a minimum of 1.05 and a maximum of 1.20. Our two checks suggest that the fitting results are *not* strongly influenced by outlier points in the data.

For the standard case ($L = 20$), there are $4 * 36 = 144$ data points, and $L + 7$ parameters. In each case, we can calculate $\alpha_{BC} = \alpha_{BA}\alpha_{AC}$. E.g. for $L = 20$ the result is $\alpha_{BC} = 1.10^{+.08}_{-.08}$. With $L = 20$, the 1σ uncertainties from Gaussian Monte Carlo trials are, for comparison with Table 3, $^{+0.9}_{-0.9}$ days for t_{AC}, $^{+1.1}_{-1.1}$ days for t_{BA}, $^{+1.4}_{-1.3}$ days for t_{BC}, $^{+.13}_{-.14}$ for r_{ABC}, $^{+.07}_{-.06}$ for α_{AC}, $^{+.04}_{-.04}$ for α_{BA}, and $^{+.07}_{-.07}$ for α_{BC}. The 95% confidence limits from bootstrap Monte Carlo trials are, also for the $L = 20$ case, $^{+2.0}_{-2.2}$ days for t_{AC}, $^{+2.9}_{-3.2}$ days for t_{BA}, $^{+3.3}_{-3.8}$ days for t_{BC}, $^{+.31}_{-.41}$ for r_{ABC}, $^{+.16}_{-.20}$ for α_{AC}, $^{+.10}_{-.12}$ for α_{BA}, and $^{+.15}_{-.19}$ for α_{BC}. For this standard case, Figure 1 shows the quasar components A ($\star$), B ($\bullet$), and C ($\circ$) (including the final point in each light curve, which was excluded from the fitting). All have been corrected in each observation only by the error component which is common to all the quasar components and to *B, as reconstructed by the fitting. Other than this A is shown as observed (except for a vertical shift to have zero mean), but B and C are shifted and scaled according to the values of m_{AC}, m_{BA}, t_{AC}, t_{BA}, α_{AC}, and α_{BA}. Also shown are the reconstructed signal (solid line) and the input used in the Monte Carlo trials (dotted line). Figures 2 and 3 show one dimensional χ^2 plots, as a function of t_{BC} and r_{ABC}, respectively. In each plot, at every point the parameter shown is fixed and χ^2 is minimized with respect to all other parameters. The plots do not show any strong local minima that could be confused with the global minimum. The formal 1σ uncertainties derived from these curves are 1.0 day for t_{BC} and .12 for r_{ABC}. Figure 4 shows a two dimensional χ^2 plot as a function of t_{AC} and t_{BA}, around the minimum (marked $\times$). The same χ^2 contours are also shown as a function of t_{BC} and r_{ABC}. Note that the result of SCH (marked $\circ$) is outside even the outermost contour, which delineates the formal 99.99% confidence level. The figure clearly shows that the main disagreement of the present results with SCH is in the value of r_{ABC}, while

the values of t_{BC} are consistent with each other.

We adopt the $L = 20$ results and bootstrap uncertainties, since they are compatible with the values for the other L to about 1σ. Thus $t_{BC} = 25.0^{+1.5}_{-1.7}$ days, and Tables 2 and 3 indicate that this 6% uncertainty (at 68% confidence) is a reasonable estimate. Our value used with lens models reduces the induced H_0 only by 5% relative to the SCH value. On the other hand, r_{ABC} varies fairly strongly with different assumptions, and is only weakly constrained at $r_{ABC} = 1.13^{+.18}_{-.17}$. This result is close to the values around 1.4 predicted by lens models, but the uncertainty is too large to be able to decide among different types of models (Keeton & Kochanek 1997). The fitting also recovers $m_{AC} = 2.033 \pm .005$, $m_{BA} = -2.534 \pm .007$, and $m_{BC} = -.501 \pm .008$, which yield variation-subtracted magnification ratios for the mean flux. These agree with SCH and also with the flux ratios of Kristian et al. (1993), since the quasar does not vary much over the time scale of the time delays. Our extremely accurate magnification ratios are not useful for lens modelling, since they are still likely to be greatly altered by microlensing, as suggested by the variation ratios.

Regarding the variation ratios, $\alpha_{BC} = 1.10^{+.08}_{-.08}$ is consistent with 1, while $\alpha_{AC} = 1.39^{+.07}_{-.08}$ is greater than 1 and $\alpha_{BA} = .79^{+.05}_{-.06}$ is less than 1, both at $4 - 5\sigma$. These values are also roughly consistent with Table 2. To make perhaps a more direct test of the significance of this result, we also perform Monte Carlo tests on input which has variation ratios equal to 1, but they are allowed to vary in the fitting. The result indicates that if the variation ratios were really 1, we would measure $\alpha_{AC} = 1.00^{+.07}_{-.07}$ ($^{+.14}_{-.17}$ at 95% confidence) and $\alpha_{BA} = 1.00^{+.10}_{-.10}$ ($^{+.19}_{-.23}$ at 95% confidence), so in this sense the $L = 20$ results for α_{AC} and α_{BA} are significantly different from 1 at 5σ and 2σ, respectively. As discussed in §2, this may indicate that the quasar optical emission region must be of order 1000 AU in linear dimension.

4. Conclusions

We have developed a method for determining time delays among light curves of multiple images of a gravitational lens. The method constructs a simple model for the actual source variation, using interpolation between a number of equally spaced values. It then performs a combined χ^2 minimization by fitting all of the light curves to this model simultaneously, which is similar to the method of Press et al. (1992a, b). The ability to vary the basic parameters of the model over a large range lends robustness to our method. Most of the parameters are linear and so the χ^2 minimization is easily done. In addition to the time delays, the other non-linear parameters are relative variation ratios, which account for different fractional variation in flux for different images. We interpret this physically as evidence for differential microlensing, i.e. a different magnification due to microlensing for the varying region from the region giving rise to the mean flux.

Applying our method to the light curves of PG1115+080 observed by SCH, we find a value of $25.0^{+3.3}_{-3.8}$ days (95% confidence) for the delay between components B and C, and a ratio t_{AC}/t_{BA} for the two smaller delays of $1.13^{+.18}_{-.17}$ (68% confidence). Unlike SCH, we include correlated measurement errors as well as the above mentioned variation ratios in the analysis. Our result for t_{BC} agrees with SCH, but the ratio r_{ABC} does not. Our result for r_{ABC} does agree with lens models, but we find that with the present data it cannot be derived accurately enough to help in fitting lens models. For the variation ratios, we

find $\alpha_{AC} = 1.39^{+.16}_{-.20}$ and $\alpha_{BA} = .79^{+.10}_{-.12}$ (95% confidence), each indicating differential microlensing at a significance of $4-5$ times our estimated 1σ uncertainties. If confirmed as the data accumulates, this would imply that the size of the quasar optical emission region is of order 1000 AU, for microlenses of $\langle M \rangle = 0.1 M_\odot$. Further data may also allow a determination of the time variation of the two microlensing magnifications.

I thank Paul Schechter for suggesting this project and for helpful advice, Ed Bertschinger for encouragement and useful comments, and Doug Richstone and Ned Wright for valuable comments. This work was supported by NASA grant NAG5-2816 and NSF grant AST-9529154.

REFERENCES

Corbett, E. A., Browne, I. W. A., & Wilkinson, P. N. 1996, in Astrophysical Applications of Gravitational Lensing, Proceedings IAU Symposium 173, ed. C. S. Kochanek & J. N. Hewitt (Dordrecht: Kluwer), 37

Falco, E. E., Gorenstein, M.V., & Shapiro, I. I. 1985, ApJ, 289, L1

Falco, E. E., Shapiro, I. I., Moustakas, L. A., & Davis, M. 1997, preprint astro-ph/9702152

Gould, A., & Miralda-Escudé, J. 1997, preprint astro-ph/9612144

Grogin, N. A., & Narayan, R. 1996a, ApJ, 464, 92

Grogin, N. A., & Narayan, R. 1996b, erratum, ApJ, 473, 570

Haarsma, D. B., Hewitt, J. N., Lehár, J., & Burke, B. F. 1997, ApJ, 479, 102

Houde, M. & Racine, R. 1994, AJ, 107, 466

Irwin, M. J., Webster, R. L., Hewett, P. C., Corrigan, R. T., & Jedrzejewski, R. I. 1989, AJ, 98, 1989

Keeton, C. R., & Kochanek, C. S. 1997, preprint astro-ph/9611216

Kochanek, C. S. 1991, ApJ, 373, 354

Kristian, J. et al. 1993, AJ, 106, 1330

Kundić, T., Turner, E. L., Colley, W. N., Gott, J. R., Rhoads, J. E., Wang, Y., Bergeron, L. E., Gloria, K. A., Long, D. C., Malhorta, S., & Wambsganss, J. 1997, preprint astro-ph/9610162

Narayan, R. 1991, ApJ, 378, L5

Press, W. H., Rybicki, G. B., & Hewitt, J. N. 1992a, ApJ, 385, 404

Press, W. H., Rybicki, G. B., & Hewitt, J. N. 1992b, ApJ, 385, 416

Press, W. H., Teukolsky, S. A., Vetterling, W. T., & Flannery, B. P. 1992c, Numerical Recipes in Fortran: The Art of Scientific Computing, Sec. Edition (New York: Cambridge Univ. Press)

Refsdal, S. 1964, MNRAS, 128, 307

Refsdal, S. 1966, MNRAS, 132, 101

Schechter, P. L., et al. 1997, ApJ, 475, 85 (SCH)

Schild, R. E. 1996, ApJ, 464, 125

Van Ommen, T. D., Jones, D. L., Preston, R. A., & Jauncey, D. L. 1995, ApJ, 444, 561

Walsh, D., Carswell, R. F., & Weymann, R. J. 1979, Nature, 279, 381

Wambsganss, J., & Paczyński, B. 1994, AJ, 108, 1156

Wambsganss, J., Paczynski, B., & Schneider, P. 1990, ApJ, 358, 33L

Weymann, R. J., Latham, D., Angel, J. R. P., Green, R. F., Liebert, J. W., Turnshek, D. E., & Tyson, J. A. 1980, Nature, 285, 641

Witt, H. J., Mao, S., & Schechter, P. L. 1995, ApJ, 443, 18

Young, P., Deverill, R. S., Gunn, J. E., Westphal, J. A., & Kristian, J. 1981, ApJ, 244, 723

Table 1. Single quasar component fitting

L	ndof	A, $\bar{\chi}^2$	B, $\bar{\chi}^2$	C, $\bar{\chi}^2$
10	61	0.66	1.15	0.66
20	51	0.58	0.78	0.58
30	41	0.67	0.74	0.67

Table 2. Fitting of quasar components in pairs

L	ndof	$\bar{\chi}^2$	time delay [days]	var ratio
		BC components		
10	94	1.77	$25.0^{+1.7}_{-1.8}$	$1.07^{+.09}_{-.09}$
20	84	1.54	$25.3^{+2.3}_{-2.0}$	$1.09^{+.09}_{-.09}$
30	74	1.03	$26.7^{+1.8}_{-1.8}$	$1.03^{+.06}_{-.07}$
		AC components		
10	94	1.27	$11.0^{+0.9}_{-0.9}$	$1.35^{+.06}_{-.06}$
20	84	1.06	$11.0^{+0.9}_{-0.9}$	$1.52^{+.09}_{-.08}$
30	74	0.98	$12.3^{+1.3}_{-1.0}$	$1.40^{+.09}_{-.10}$
		BA components		
10	94	2.38	$11.7^{+2.0}_{-2.0}$	$0.74^{+.05}_{-.05}$
20	84	1.48	$6.75^{+1.7}_{-1.5}$	$0.61^{+.05}_{-.04}$
30	74	1.06	$7.22^{+1.2}_{-1.2}$	$0.46^{+.03}_{-.03}$

Table 3. Fitting of the three quasar components

Input*	ndof	$\bar{\chi}^2$	t_{AC} [days]	t_{BA} [days]	t_{BC} [days]	r_{ABC}	α_{AC}	α_{BA}
$L = 10$	127	1.83	$12.5^{+0.9}_{-0.9}$	$14.0^{+1.6}_{-1.6}$	$26.5^{+1.7}_{-1.7}$	$0.89^{+.12}_{-.13}$	$1.45^{+.06}_{-.06}$	$.80^{+.05}_{-.05}$
$L = 20$	117	1.60	$13.3^{+0.9}_{-1.0}$	$11.7^{+1.5}_{-1.6}$	$25.0^{+1.5}_{-1.7}$	$1.13^{+.18}_{-.17}$	$1.39^{+.07}_{-.08}$	$.79^{+.05}_{-.06}$
$L = 30$	107	1.38	$14.9^{+1.4}_{-1.3}$	$10.6^{+1.3}_{-1.3}$	$25.5^{+1.8}_{-1.6}$	$1.41^{+.27}_{-.25}$	$1.43^{+.08}_{-.08}$	$.72^{+.04}_{-.05}$
$\sigma_n = 4$	117	2.27	13.0	11.8	24.8	1.10	1.38	.80
$\sigma_n = 8$	117	1.34	13.4	11.7	25.1	1.15	1.39	.79
$f_1 = 0$	117	2.01	12.8	11.4	24.2	1.12	1.34	.80
$f_2 = 0$	117	2.13	12.8	11.8	24.6	1.08	1.38	.81
cubic	117	1.56	13.4	11.9	25.2	1.13	1.39	.80
linear	117	1.55	13.5	11.7	25.1	1.15	1.40	.79
SCH-like	84	1.61	$8.9^{+1.7}_{-1.6}$	$11.9^{+2.8}_{-2.5}$	$20.9^{+2.9}_{-2.6}$	$0.75^{+.26}_{-.29}$	1	1

*See text.

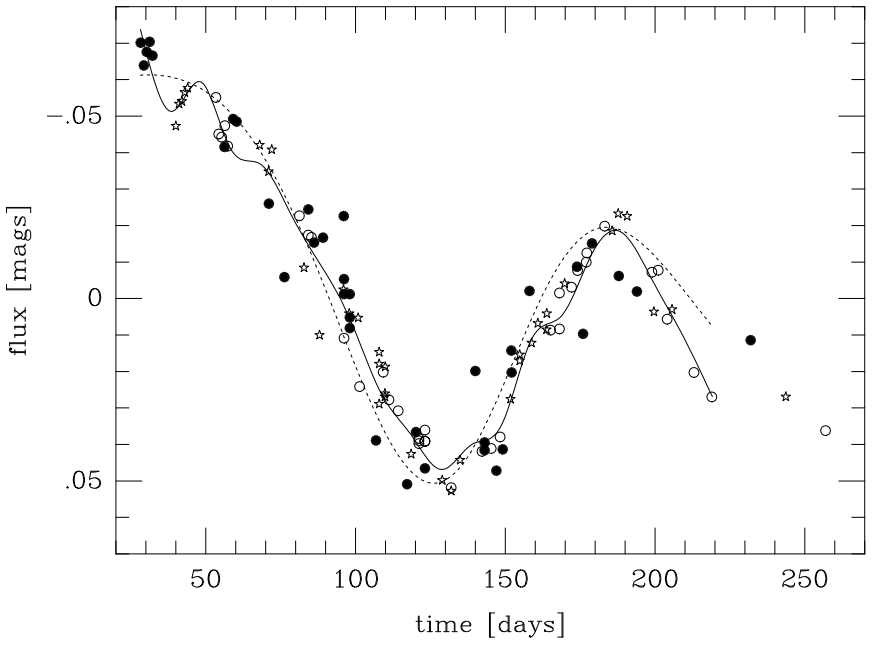

Fig. 1.— Light curves for components A (⋆), B (•), and C (◦). B and C have been shifted to match A, and all have been partly corrected for errors (see text). Also shown are the reconstructed signal (solid line), the input used in Monte Carlo trials (dotted line), and the final point in each light curve, which was excluded from the fitting.

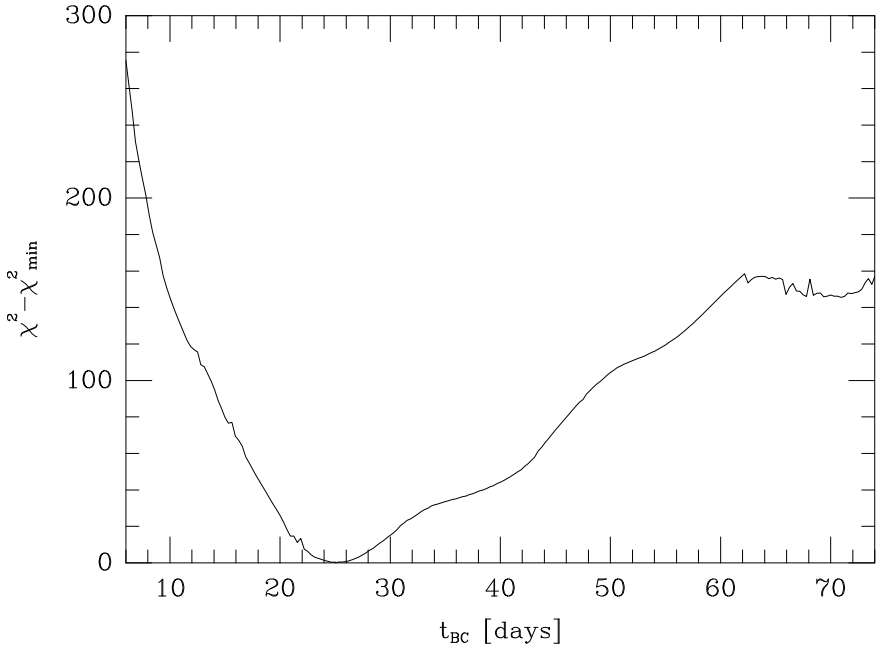

Fig. 2.— Value of χ^2 versus assumed delay t_{BC}, relative to the χ^2 value at its global minimum.

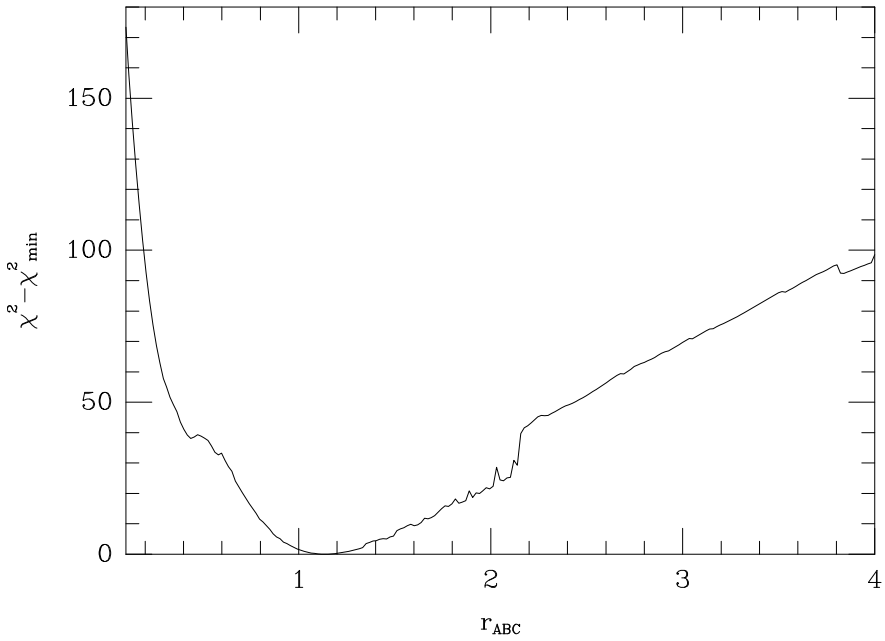

Fig. 3.— Value of χ^2 versus assumed ratio r_{ABC}, relative to the χ^2 value at its global minimum.

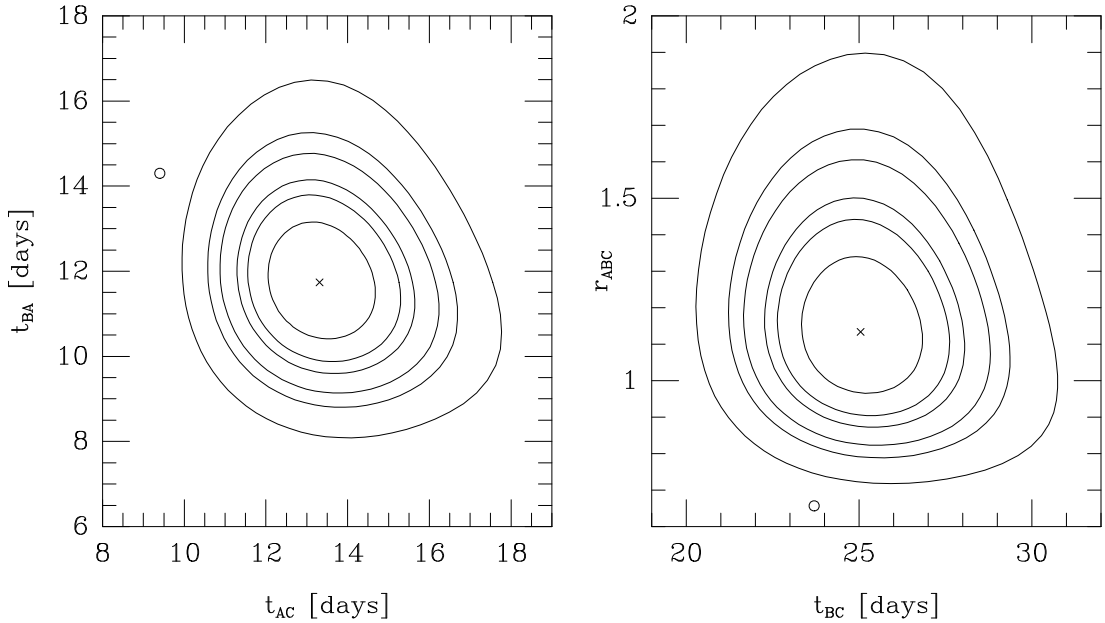

Fig. 4.— χ^2 contours in the t_{AC}, t_{BA} plane (left) and in the t_{BC}, r_{ABC} plane (right). The point marked $\times$ is $\chi^2 = 187$, the global mimimum. The contours are drawn at $\Delta\chi^2$ =2.30, 4.61, 6.17, 9.21, 11.8 and 18.4, the 1σ, 90%, 2σ, 99%, 3σ and 99.99% confidence levels for two parameters. The point marked $\circ$ is the SCH result.